Computational Model of Ductal Carcinoma *In Situ*: The Effects of Contact Inhibition on Pattern Formation

Seth D. Shumate* and Magda El-Shenawee, *Senior Member, IEEE*

***Abstract*—The computational model presented in this paper focuses on modeling ductal carcinoma *in situ* (DCIS), which is the most commonly detected preinvasive form of breast cancer. The model aims to understand the biological mechanisms and resultant growth dynamics of DCIS. The cellular automaton model based on observed phenotypic characteristics of DCIS emphasize the important role of contact inhibition on lesion pattern formation. Computer simulations resembled the cribriform, micropapillary, solid, and comedo patterns of DCIS. The model has led to insights about the progression of the preinvasive disease such as possible explanations for coexisting micropapillary and cribriform patterns commonly found through histological analyses.**

***Index Terms*—Cellular automata, ductal carcinoma *in situ* (DCIS), pattern formation, theoretical biology.**

I. Introduction

THE PROGRESSION of ductal carcinoma *in situ* (DCIS) to invasive ductal carcinoma (IDC) is still largely unknown. IDC represents 75% of breast cancer incidence in the United States. Normal function of the mammary parenchyma is a tightly controlled process. The ducts of the mammary gland are composed of an inner layer of epithelial cells surrounded by a myoepithelial layer and then by a basement membrane (see Fig. 1). Mutational abnormalities in the epithelial cell layer or its progenitor cells lead to the excessive proliferation known as DCIS and IDC. While the exact natural history of ductal carcinoma is still unclear, specifically regarding the progression from its *in situ* to its invasive form, several classifications of the disease have been established [1], [2].

Works explaining the underlying causes for the different DCIS morphologies have not been found in the literature. One reason for the ambiguous nature of DCIS is that when found, the affected area is removed for the obvious benefits to the patient's health. This has made it necessary to study the disease with less realism using *in vitro* methods, histological analyses, and animal models. The emerging field of theoretical biology, a mixture of computer science, mathematics, and biology, is emerging as a standard method for studying tumorigenesis. There are many challenges facing each method, which is why a combined effort must be realized in order to understand the complexities of DCIS and IDC.

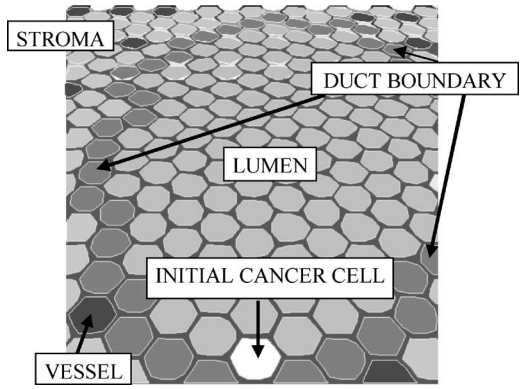

Fig. 1. Initially, the local tissue environment involves the duct boundary composed of healthy epithelial cells, blood vessels, stroma, a cancer seed, and duct lumen.

Morphologically, DCIS lesions are classified as cribriform, micropapillary, solid, and comedo. Cross sections of a duct containing cribriform DCIS present a pattern likened to swiss cheese due to characteristic holes left unfilled by the neoplastic cells. Micropapillary patterns are often found in the same duct system with cribriform DCIS [3], [4]. Both types can have associated clinging patterns in which cancerous cells adhere to the walls of the duct. It has not been established whether varying pattern types found in the same duct are of differing genotypes or merely behave differently due to the heterogeneity in the microenvironment. Both solid and comedo DCIS fill the duct, but comedo DCIS contains central areas of dead cells known as the necrotic core. These cells die due to diffusion limitations of essential nutrients.

Several mathematical and computational models have been proposed, which attempt to describe different facets of DCIS [5]–[9]. Franks *et al*. [5]–[7] represented the tumor as a Newtonian fluid growing in the duct. The growth of the tumor mass was dependent on nutrient diffusion, and the tumor secreted matrix degradative enzymes that decreased the basement membrane's resistance to dilation [5]–[7]. In this case, tumor cells were not modeled explicitly, excluding important aspects such as cell–cell interactions. In another model, Xu modified a framework proposed by Byrne *et al*. to tumor growth within a cylinder [8]. This model reported that the patterns observed in DCIS

Manuscript received December 18, 2007; revised April 8, 2008. First published September 16, 2008; current version published May 22, 2009. This work was supported in part by the National Science Foundation under Grant ECS 0524042, in part by the Arkansas Biosciences Institute (ABI), and in part by the National Science Foundation GK-12 Fellowship Program. *Asterisk indicates corresponding author.*

*S. D. Shumate was with the Microelectronics-Photonics Program, University of Arkansas, Fayetteville, AR 72701 USA. He is now with the University of Dundee, Dundee DD1 1HG, U.K. (e-mail: sshumat@uark.edu).

M. El-Shenawee is with the Department of Electrical Engineering, University of Arkansas, Fayetteville, AR 72701 USA (e-mail: magda@uark.edu).

Digital Object Identifier 10.1109/TBME.2008.2005638

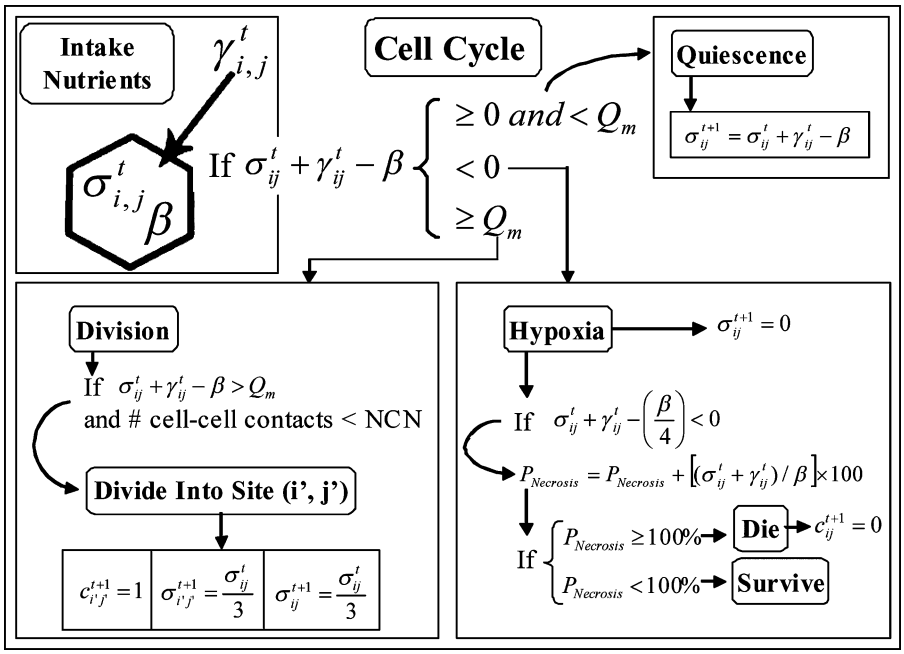

Fig. 2. Cancer cell cycle flowchart shows the three possible nutrient-dependent processes that the cell can undergo during one iteration. When a cell divides, the daughter cell prefers to enter a site that has an adequate number of neighbors for contact inhibition. The other daughter cell remains at site (i,j).

were based solely on nutrient diffusion and uptake by the neoplasm [8]. In this model, tumor cells were also not explicitly considered since the tumor distribution was represented by nutrient gradients [8]. The third model, as proposed by Bankhead *et al*., while using different cell types modeled on an individual level, focused on analyzing different progenitor cell hierarchies as have been proposed for mammary stem cells [9]. This model incorporated an interesting mutational system and used a more biologically based approach to modeling DCIS than the others, yet did not emphasize specific cell–cell interactions or pattern formation.

While each of the aforementioned models is unique in purpose and execution, in order to model complex behavior as seen *in vivo*, the authors believed that discrete factors should be considered. The model developed in this paper incorporates specific characteristics of DCIS such as intercellular interactions, nutrient consumption, hypoxia, a basic cell cycle, certain mutational assumptions, characteristic extraductal vascularization, and dimensionally accurate necrosis in order to reproduce clinically observed DCIS patterns.

II. Methodology

A. Discretization and Nutrient Diffusion

The simulated duct, made up of only a single layer of normal epithelial cells acting as the duct boundary, is placed at the center of a 300 × 300 hexagonal grid. Each cell has a diameter of 10 μm, and duct diameters in simulations shown here will be either 440 or 900 μm in order to be consistent with the range of duct sizes *in vivo* [5]–[7]. The myoepithelial layer and basement membrane are not included here, but will be involved explicitly in future work modeling the progression from DCIS to IDC. A generic nutrient flows from 29% of the extraductal sites, which corresponds to the microvessel density reported by Naccarato *et al*. for normal mammary tissue [11]. The capillary distribution was kept constant for the simulations presented.

The nutrient diffusion and nutrient uptake system was modified from a model proposed by Sansone *et al*. to work on an individual cell level using a hexagonal lattice. In the original model, every point on the 2-D Cartesian grid could contain many cells of differing types, which inherently limits modeling cell–cell interactions [11]. The nutrients at any site diffuse between the six neighboring sites based on concentration as described by

$$p^{t+1}_{ij} = p^t_{ij} + \sum_{i'j'}^{NN} (\alpha_{ij} p^t_{i'j'} - \alpha_{i'j'} p^t_{ij}) - \gamma^t_{ij} - \xi^t_{ij} + \psi^t_{ij} \quad (1)$$

where p^t_{ij} represents the nutrient level at site (i, j) at the current iterative timestep t. The nutrient diffusion coefficients α_{ij} and $\alpha_{i'j'}$ represent the relative rates at which nutrients flow through different tissues. Capillaries maintain a constant nutrient level ψ^t_{ij} that is updated for every iteration. The normal stromal tissue sites also uptake nutrients at a constant rate ξ^t_{ij}, which is normally less than γ^t_{ij}. This corresponds to the increased rate at which cancerous cells uptake nutrients, and is given as

$$\gamma^t_{ij} = \Gamma \left[1 - e^{\left(-p^t_{ij}/\Gamma\right)}\right] \quad (2)$$

where Γ is the saturation constant for nutrient transport into the cancer cell. In the article by Sansone *et al*., multiple tissue types such as bone and cartilage were included and considered to be less permeable to nutrient flow, and consequently, had lower values for α_{ij} at such sites [11]. Every cell type in this study is assigned the same nutrient diffusion coefficient. Depending on their internal nutrient level at any given iteration, cancerous cells will either remain quiescent, enter a hypoxic state, die, or divide. A flowchart for the cell cycle is given in Fig. 2. The

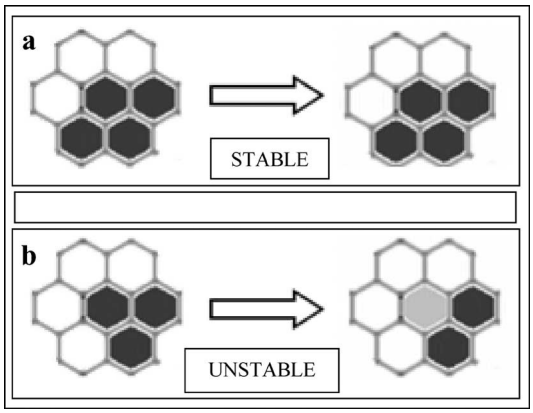

Fig. 3. If the necrotic cell is surrounded by four or more nonnecrotic cells for 200 iterations, it will be absorbed by the surrounding cancer cells and the site will become empty. White cells are cancerous, dark gray cells are necrotic, and the light gray site is luminal space.

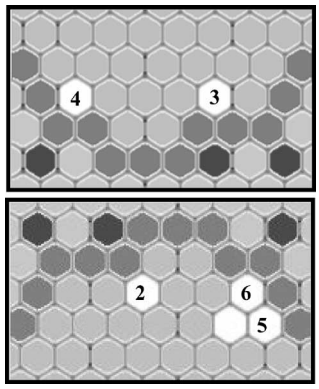

Fig. 4. Indicated cells with their corresponding NCNs are able to divide.

cancerous cells have a metabolic rate β at which the nutrients transported into the cell are used to sustain cell viability. Any nutrients not used by a cell during the iteration are added to the cell's nutrient storage σ_{ij}^t.

B. Hypoxia and Necrosis

In this model, random apoptosis is not considered. Normal hypoxia-induced apoptosis has been shown to be evaded by some breast cancer cells [12]. For the simulated cases shown later in this paper, necrosis will be the only form of cell death. Before cell death occurs, cells can enter a hypoxic state in which they require only 0.25β. Once the internal nutrients available to a cell drop below 0.25β, the cell will become a necrotic entity

$$\sigma_{ij}^t + \gamma_{ij}^t - \left(\frac{\beta}{4}\right) < 0. \tag{3}$$

Once a cell dies, it can be absorbed into its surrounding if it has more than three nonnecrotic neighboring sites. Otherwise, the site will remain necrotic. As illustrated in Fig. 3, the necrotic cell in the center site in example (a) only has three nonnecrotic neighbors, while the central necrotic site in example (b) has four. After 200 iterations of these configurations, only the necrotic site in example (b) will become a luminal site, open to occupation by a cancer cell.

C. Cell Division

Cancer cell division is governed by an algorithm for contact inhibition as well as a nutrient dependence expressed by

$$\sigma_{ij}^t + \gamma_{ij}^t - \beta > Q_m \tag{4}$$

where Q_m is the threshold level of nutrients required for cell division. When (4) is satisfied, then the number of surrounding sites occupied by either cancer or normal epithelial cells determines whether or not the cell's division will be contact inhibited. This model represents the role of E-Cadherin in epithelial cell contact inhibition. E-Cadherin is a cell–cell adhesion molecule, and its expression in DCIS has been shown to be significantly decreased, especially in the high-grade comedo type [2]. As a consequence of decreased expression of E-Cadherin, DCIS cells become less sensitive to contact inhibition [13]. Other mechanisms by which a cell's sensitivity decreases in response growth-inhibitory cell–cell contacts may exist, but are not explicitly represented in the DCIS model. The contribution of this study is in the incorporation of these two ideas in a concise fashion in order to provide an *in silico* experiment to determine the possible effects of contact inhibition on DCIS pattern formation. Otherwise, direct observation via *in vitro* or animal models using techniques to tightly control a continuous decrease in cell response to contact inhibition would be required. To the best of the authors' knowledge, such a sophisticated system has not been developed for studying DCIS pattern formation.

The physiological observations are simulated algorithmically by considering the microenvironment in two dimensions. A hexagonal lattice was chosen over a square lattice because, like columnar epithelium, each site has six lateral neighbors with which to interact. At the beginning of a simulation, the initial cancer seed and any subsequent cancer cell is given an integer value in the range from 2 to 6. This integer will be referred to as the neighboring cell number (NCN). It is meant to represent the amount of expression of, or lack of response to, E-Cadherin-mediated contacts, and, in turn, the number of neighboring cells required to arrest the cell cycle. Quantitative data have not been found in the literature with which to directly correlate this system. In this sense, NCN values and probability combinations were devised *ad hoc* based on the 2-D nature of the modeling system.

In 2-D terms, the normal epithelial cell layer, as shown in Fig. 4, consists of cells fully expressing E-Cadherin, and thus, require only two neighboring cells, or NCN $= 2$, to be inhibited from dividing. Accordingly, if the cancer cells have a decreased level of E-Cadherin expression, or lack of response to it, their NCN numbers will be higher. Fig. 4 shows cells which, provided they have sufficient nutrients, are able to divide into empty neighboring sites so long as their NCN is greater than the number of cells surrounding them. NCN probabilities are selected between two consecutive integers or can fall directly on a single value. These probabilities will be referred to as $\text{NCN}_X = Y\%$, where Y is the probability that the NCN value for a cell at an iteration will be X. For example, in Fig. 4, the

TABLE I
CONSTANT PARAMETERS AND INITIAL VALUES USED FOR ALL SIMULATIONS

Parameter	Value	Description
α_{ij}	0.166	Nutrient diffusion coefficient for all tissue types.
ξ_{ij}^{t}	0.002 0.001	Stromal tissue nutrient intake Capillary nutrient intake
Γ	0.006	Max. nutrient intake by cancer Cells
β	0.005	Metabolic rate for cancer cells
Q_m	0.15	Mitotic nutrient threshold

cell with $\mathrm{NCN}_2 = 100\%$ is in contact with only one cell. Since its number of neighbors is less than its current NCN value, this cancer cell is not contact inhibited.

If a cell does not have enough nutrients to divide, has not entered a hypoxic state, or is inhibited by contacts with neighboring cells, then the cell will remain quiescent and the stored nutrients will increase by $(\gamma_{ij}^{t} - \beta)$. If a cell does divide, then each daughter cell will retain a third of the original cell's stored nutrients.

III. RESULTS

C++ was used to program the model, and Python scripting through the Blender–Python Advanced Programming Interface (API) was used to visualize the simulations. Each case shown here uses the same parameters as given in Table I. These parameters were fit to produce architecturally valid Comedo DCIS morphology since this pattern of DCIS is the most heavily influenced by nutrient diffusion. DCIS is typically classified into low and high grades. These classifications are based on prognostic factors such as nuclear morphology, mitotic rate, and cell differentiation. Low-grade types of DCIS include cribriform, micropapillary, and solid that are less aggressive than the high-grade, comedo type.

A. Low-Grade DCIS

The cribriform type of DCIS in histological slides contains areas where cells have not and supposedly will not invade. In Fig. 5, cribriform growth simulation is visualized unto completion after 7600 iterations. The timestep in the program does not explicitly relate to a biological time, but to the relative rates at which cells divide and nutrients diffuse. *In vivo*, cells are usually well differentiated with polarized surfaces facing the open areas. Low grade DCIS, including cribriform, was found to have a significantly higher level of E-Cadherin expression than the high-grade comedo DCIS [2]. Under histological analysis, holes as well as slits are observed for cribriform DCIS.

Fig. 5 displays a chronological view of simulated cribriform DCIS. Around $i = 2000$, some open areas have already reached stable configurations that persist to the end of the simulation. Another area can be seen forming in the upper portion of the growth. The surface cells on the left of this area are in a stable configuration; so, the peninsula of cells to the right of the open area grow from right to left to fill the area in, as can be seen in the snapshot at $i = 4000$. This pattern type is obtained during simulations with combinations of NCN_3 and NCN_4 probabilities or $\mathrm{NCN}_4 = 100\%$.

Fig. 6(a) shows simulated patterns from only varying NCN probabilities. Each of these cases is shown after 25 000 iterations, and, in general, the lower values of NCN correspond to decreased proliferation rates. This is an obvious product of the model since cells with low values of NCN, or more normal E-Cadherin levels, have fewer possible configurations where cell division is not inhibited.

The micropapillary-like structures begin, as with the other simulations, with a single cancer seed neighboring only one healthy epithelial cell. This allows a cell even with $\mathrm{NCN}_2 = 100\%$ to proliferate at least once. The patterns reach a stable configuration in relatively few iterations. In order to produce more complex micropapillary patterns as seen *in vivo*, multiple cancer seeds could have been initiated along the duct boundary. The solid pattern seen in Fig. 6(a) would appear as a case of comedo DCIS, except that the duct diameter is only 440 μm, thus providing sufficient nutrients for the central cells to survive.

B. Pattern Continuum Hypothesis

Each of the simulations discussed so far were performed under the assumption that the healthy luminal epithelial cells contribute to contact inhibition of the cancerous cells even though the apical membrane of these epithelium do not normally express E-Cadherin *in vivo*. In this case, as shown in Fig. 6(a), the cribriform patterns allow the formation of holes along the duct boundary. In the case where the healthy epithelial cells do not contribute to contact inhibition, as shown in Fig. 6(b), the cribriform holes do not form along the duct boundary, but the cancer cells cling to the sides during the evolution of the simulated lesions.

When the boundary epithelial cells in the model do not contribute to contact inhibition, which may well be the case *in vivo*, interesting behaviors arise that may explain why clinging, micropapillary, and cribriform patterns can all be observed in the same duct system. Micropapillary patterns are observed in the model when the NCN_3 probability dominates NCN_4, yet after many iterations, the duct will be filled with the cribriform pattern. Intermediate stages also show clinging behavior. Fig. 7 displays an example of this phenomenon for $\mathrm{NCN}_4 = 0.029\%$. Micropapillary projections into the lumen eventually grow toward one another, forming the stable cribriform configuration.

Under these conditions, the model indicates that it is possible for the micropapillary and cribriform types of DCIS to exist in the same duct and that the micropapillary patterns are merely immature cribriform DCIS.

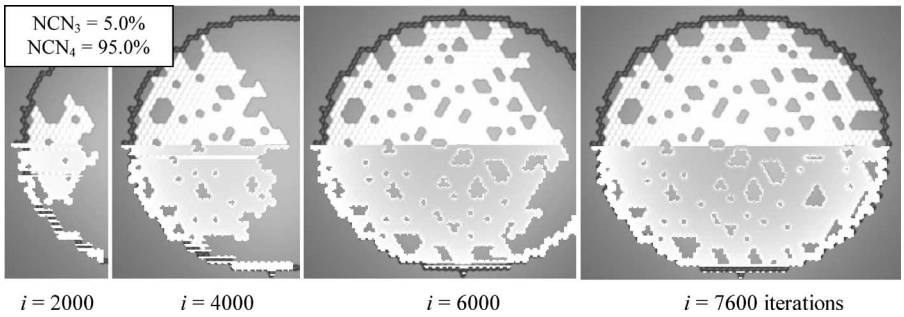

Fig. 5. DCIS growth simulation demonstrating characteristic cribriform patterns. $NCN_4 = 95\%$ and $NCN_3 = 5\%$. Nutrient distributions are superimposed over the cancer cell map. The darker regions indicate lower nutrient concentrations. Assuming that the cells are 10 μm in diameter, the duct diameter would be 440 μm.

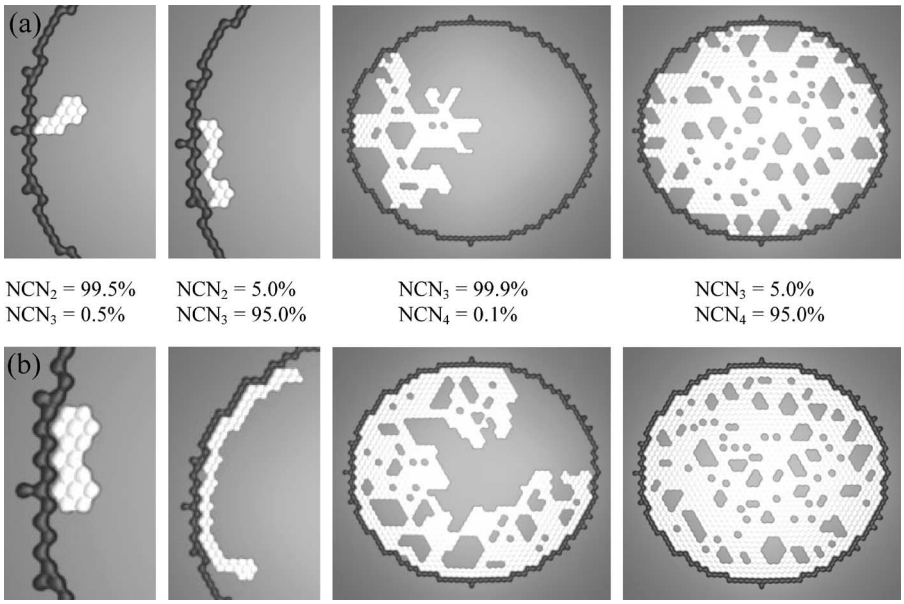

Fig. 6. Patterns simulated (from left to right): clinging, papillary, cribriform, and solid in which (a) the healthy epithelial layer contributes to contact inhibition and (b) does not contribute to contact inhibition.

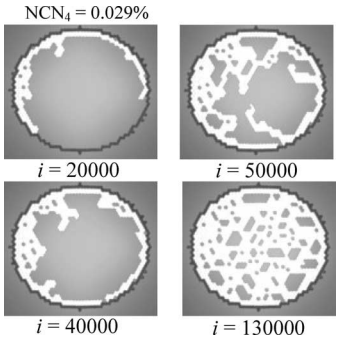

Fig. 7. When $NCN_3 \gg NCN_4$, there is a gradual progression from micropapillary patterns to a full cribriform pattern after 130 000 iterations.

C. Comedo DCIS

High-grade, Comedo DCIS contains a necrotic core surrounded by viable cells. The parameters in this model were fit to produce a necrotic core that would form after a viable rim of 315 μm, consistent with distances measured through histological image analysis [14]. When comedo DCIS forms *in vivo*, the duct is distended due to the pressure from proliferation and factors weakening the basement membrane [5], [15]. The simulation in Fig. 8 has a duct diameter of 900 μm with $NCN_6 = 100\%$. The necrotic core is composed of coagulative necrotic cells. The time at which the core starts forming and the relative rate at which necrotic cells become luminal sites are important factors in reproducing the comedo morphology. For example, if the rate of necrotic to lumen progression is lowered from 200 iterations to 100, then the core will not form fast enough to maintain the initial necrotic sites. The final result would be a central lumen with insufficient nutrients to sustain further cancer growth. If this were the behavior *in vivo*, then pressure effects from the surrounding proliferating cells would likely reduce this area. Such a pattern with an open lumen and many viable cells is not seen *in vivo*.

D. Semiquantitative Validation

In order to assess the similarity of patterns reproduced by the model with those displayed from histological slides of DCIS, a simple image-analysis method was performed. The contours

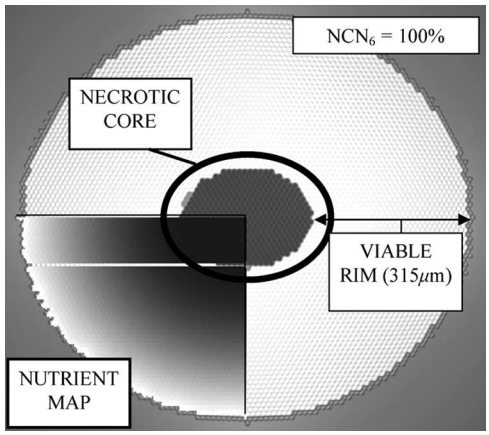

Fig. 8. Necrotic core formation begins after 315 μm and is surrounded by hypoxic and quiescent cells. As can be seen on the nutrient map in the lower left-hand corner, the rate of nutrient diffusion is not great enough to overcome the rate at which the cancer cells uptake the nutrients.

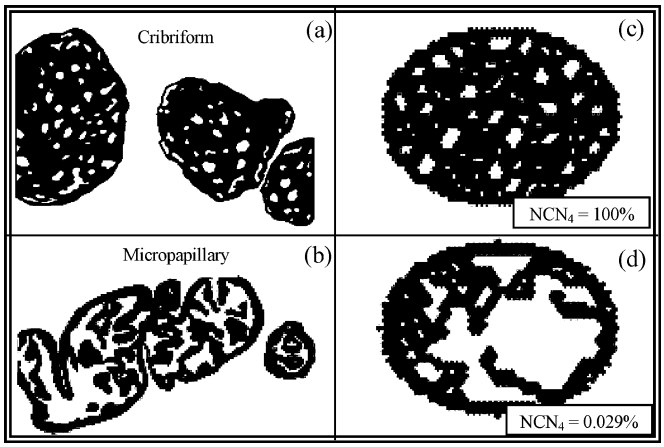

Fig. 9. Example histological slide tracings of cribriform and micropapillary lesions, (a) and (b), respectively, versus simulated results, (c) and (d). Cancer cells area is filled with black. Luminal and extraductal area is white.

of five cribriform DCIS images and ten simulated cribriform patterns were traced and compared based upon their circularity metric. Circularity (M) is often used to analyze complex shapes and is given by

$$M = \frac{4\pi A}{P^2} \tag{5}$$

where A will be defined as the number of pixels covered by the cells and P as the number of pixels forming the perimeter of cell-stroma or cell-lumen boundaries.

These values were found using Spotlight-8 Image Analysis Software (http://exploration.grc.nasa.gov/spotlight/).

A 12.2% difference was found when comparing M_{average} (0.0229) for the real example cribriform patterns with the ten simulations (0.0201). Example tracings from histological slides of cribriform [16] and micropapillary [17] patterns are shown in Fig. 9(a) and (b). Corresponding examples of simulation contours are shown in Fig. 9(c) and (d). This validation approach, while still semiquantitative, shows promise and would benefit from more histological examples.

IV. Conclusion

Pattern formation in DCIS is largely due to cell–cell interactions. A preliminary computational model for reproducing patterns such as clinging, micropapillary, cribriform, solid, and comedo DCIS is presented and discussed. The major factors governing the course of the simulations are nutrient consumption and a gradual loss of contact inhibition related to E-Cadherin expression, or an implicit lack of response to contact inhibition. Based on the model presented here, two possibilities arise to explain the relationship between the low-grade micropapillary and cribriform patterns of DCIS. They are either separate entities within the same duct system or the micropapillary portions of the lesion are simply not fully grown cribriform configurations. This could be determined experimentally through the histological analysis of whole ductal systems affected by DCIS, where the micropapillary patterns and cribriform patterns are present and their respective physical locations and molecular fingerprints are studied. If the model is correct, then such an analysis could lead to determining approximate starting locations, leading to a more accurate account of the natural history of some types of DCIS.

The results from this model, although limited by fixed hexagonal geometry, give a realistic portrait of the morphological history of DCIS from a single cell to micropapillary, cribriform, solid, and comedo patterns. This model is a simplistic version of the actual *in vivo* processes responsible for the formation of DCIS lesions.

Future work will include modeling the progression to invasion, inclusion of growth promoting and inhibiting factors, the effects of the immune system, variable cell geometry, and biomechanical processes in both 2-D and 3-D.

Acknowledgment

The authors would like to thank Dr. D. Rhoads, the Director of the Cell and Molecular Biology (CEMB), University of Arkansas, Fayetteville, for his valuable comments and suggestions on the manuscript.

References

[1] B. Erbas, E. Provenzano, J. Armes, and D. Gertig, "The natural history of ductal carcinoma *in situ* of the breast: A review," *Breast Cancer Res. Treat.*, vol. 97, pp. 135–144, 2006.

[2] S. K. Gupta, A. G. Douglas-Jones, B. Jasani, J. M. Morgan, M. Pignatelli, and R. E. Mansel, "E-Cadherin (E-cad) expression in duct carcinoma *in situ* (DCIS) of the breast," *Virchows Arch.*, vol. 430, pp. 23–28, 1997.

[3] A. S. Y. Leong, R. T. Sormunen, S. Vinyuvat, R. W. Hamdani, and C. Suthipintawong, "Biologic markers in ductal carcinoma *in situ* and concurrent infiltrating carcinoma," *Amer. J. Clin. Pathol.*, vol. 115, pp. 709–718, 2001.

[4] M. J. Van de Vijver and H. Peterse, "The diagnosis and management of preinvasive breast disease: Pathological diagnosis—Problems with existing classifications," *Breast Cancer Res.*, vol. 5, pp. 269–275, 2003.

[5] S. J. Franks, H. M. Byrne, J. C. E. Underwood, and C. E. Lewis, "Biological inferences from a mathematical model of comedo ductal carcinoma *in situ* of the breast," *J. Theor. Biol.*, vol. 232, pp. 523–543, 2005.

[6] S. J. Franks, H. M. Byrne, J. R. King, J. C. E. Underwood, and C. E. Lewis, "Modeling the early growth of ductal carcinoma *in situ*," *J. Math. Biol.*, vol. 47, pp. 24–52, 2003.

[7] S. J. Franks, H. M. Byrne, H. Mudhar, J. C. E. Underwood, and C. E. Lewis, "Modeling the growth of comedo ductal carcinoma *in situ*," *Math. Med. Biol.*, vol. 20, pp. 277–308, 2003.

[8] Y. Xu, "A free boundary problem model of ductal carcinoma *in situ*," *Discr. Continuous Dynam. Syst.—Ser. B*, vol. 4, pp. 337–348, 2004.
[9] A. Bankhead, III, N. S. SMagnuson, and R. B. Heckendorn, "Cellular automaton simulation examining progenitor hierarchy structure effects on mammary ductal carcinoma *in situ*," *J. Theor. Biol.*, vol. 246, pp. 491–498, 2007.
[10] A. G. Naccarato, P. Viacava, G. Bocci, G. Fanelli, P. Aretini, A. Lonobile, G. Montruccoli, and G. Bevilacqua, "Definition of the microvascular pattern of the normal human adult mammary gland," *J. Anat.*, vol. 203, pp. 599–603, 2003.
[11] B. C. Sansone, P. P. Delsanto, M. Magnano, and M. Scalerandi, "Effects of anatomical constraints on tumor growth," *Phys. Rev. E.*, vol. 64, no. 2, pp. 21903-1–21903-8, 2001.
[12] G. Acs, M. Chen, X. Xu, P. Acs, A. Verma, and C. Koch, "Autocrine erythropoietin signaling inhibits hypoxia-induced apoptosis in human breast carcinoma cells," *Cancer Lett.*, vol. 214, no. 2, pp. 243–251, 2004.
[13] B. St. Croix, C. Sheehan, J. W. Rak, V. A. Florenes, J. M. Slingerland, and R. S. Kerbel, "E-Cadherin-dependent growth suppression is mediated by the cyclin-dependent kinase inhibitorn p27KIP1," *J. Cell Biol.*, vol. 142, no. 2, pp. 557–571, 1998.
[14] N. A. Mayr, J. J. Staples, R. A. Robinson, J. E. Vanmetre, and D. H. Hussey, "Morphometric studies in intraductal breast carcinoma using computerized image analysis," *Cancer*, vol. 67, no. 11, pp. 2805–2812, 1991.
[15] G. Bussolati, M. Bongiovanni, P. Cassoni, and A. Sapino, "Assessment of necrosis and hypoxia in ductal carcinoma *in situ* of the breast: Basis for a new classification," *Virchows Arch.*, vol. 437, pp. 360–364, 2000.
[16] Fig. 86-4 (LP) Cribriform Pattern. (2008). [Online]. Available: http://pathology. class.kmu.edu.tw/ch10/slide86.htm
[17] (2008). [Online]. Available: http://tgmouse.compmed.ucdavis.edu/jensen-mamm 2000/dcis-6/dcis-4.htm

Seth D. Shumate received the B.A. degree in physics and Spanish from Hendrix College, Conway, AR, in 2006, and the M.S. degree in microelectronics photonics from the University of Arkansas, Fayetteville, in 2008.

From 2006 to 2007, he was a Research Assistant with the Computational Electromagnetics Group, University of Arkansa. From 2007 to 2008, he was a National Science Foundation (NSF) GK-12 Fellow. He is currently a Visiting Scholar at the University of Dundee, Dundee, U.K., supported by the NSF International Research and Education in Engineering (IREE) Program. His current research interests include computational biology, specifically studying various facets of ductal carcinoma *in situ*.

Magda El-Shenawee (M'91–SM'02) received the B.S. and M.S. degrees in electrical engineering from Assiut University, Assiut, Egypt, and the Ph.D. degree in electrical engineering from the University of Nebraska–Lincoln, Lincoln, in 1991.

During 1992, she was a Research Associate with the Center for Electro-Optics, University of Nebraska, where she worked on the problem of enhanced backscatter phenomena. During 1994, she was a Research Associate at the National Research Center, Cairo, Egypt, and during 1997, she was a Visiting Scholar at the University of Illinois, Urbana-Champaign. In 1999, she joined the Multidisciplinary University Research Initiative (MURI) Team, Northeastern University, Boston, MA. She is currently an Associate Professor in the Department of Electrical Engineering, University of Arkansas, Fayetteville. Her current research interests include breast cancer detection, computational inverse problems, microwave imaging, rough surface scattering, computational electromagnetics, subsurface sensing of buried objects, buried mines under rough ground, numerical methods, and microstrip circuits.

Dr. El-Shenawee is a member of the Eta Kappa Nu Electrical Engineering Honor Society.